LOS ALAMOS SCIENTIFIC LABORATORY
OF THE UNIVERSITY OF CALIFORNIA ○ LOS ALAMOS NEW MEXICO

QUARTERLY STATUS REPORT OF THE LASL
CONTROLLED THERMONUCLEAR RESEARCH PROGRAM
FOR PERIOD ENDING AUGUST 20, 1960

LEGAL NOTICE

LOS ALAMOS SCIENTIFIC LABORATORY
OF THE UNIVERSITY OF CALIFORNIA   LOS ALAMOS   NEW MEXICO

REPORT COMPILED: September 1960

REPORT DISTRIBUTED: September 30, 1960

QUARTERLY STATUS REPORT OF THE LASL

CONTROLLED THERMONUCLEAR RESEARCH PROGRAM

FOR PERIOD ENDING AUGUST 20, 1960

Compiled and edited

by

Samuel Glasstone

From reports written by members of P Division

SHERWOOD PROGRAM QUARTERLY REPORT

SUMMARY

1. In the entropy trapping (picket fence) experiment the plasma
density at the input cusp was increased by moving the gun closer to the P.F.
and increasing the amount of neutral gas admitted to the gun. As a result,
the input cusp has been opened to $\beta = 1$ at 2000 gauss and a $\beta = 1$ region
contained for $\sim$ 30 μsec. The contained plasma appears to be uncomfortably
close to the chamber walls. A larger apparatus in the form of a caulked
picket fence is being designed to remedy this difficulty.

2. In the skew trapping experiment measurements show complete
reflection of the off-axis input beam by the far mirror. A contained beam
has not been observed. However, there is evidence that projecting portions
of the vacuum chamber seriously intercept the beam.

3. Potential probes in a hydromagnetic gun have been used to measure
the induced radial voltage as the sheath sweeps B_θ past the probe. The
plasma velocity deduced from this voltage and the magnitude of B_θ is in
excellent agreement with direct measurements. Differential probe measurements
show that the radial voltage drop along the sheath occurs mostly within
3 mm of the center electrode, indicating a cathode drop similar to that of
classical glow discharges.

4. The large toroidal discharge, Perhapsatron S-5 Zeus, has been put
into successful operation. Measurements show that the pinch current agrees

approximately with that predicted on the basis of previous experience. Neutron bursts of about 10^8 have been obtained, but tests at voltages higher than 17.5 kv were terminated by failure of the quartz torus.

5. The microwave scattering experiment has been improved by the application of a microwave phase shift interferometer in order to measure the electron density. The measurements show that the density attained so far is too low to produce a detectable scattered signal in the receiver. Steps are being taken, therefore, to improve the rf ionization system. Parts are being ordered to enable a search for radiation scattered by collective ion oscillations.

6. A technique has been developed for measuring the electron temperature as a function of time on a single discharge in Scylla. It is found that the temperature during a given half-cycle of compression field peaks later than B_z, as would be expected from a simple model of adiabatic compression and collisional energy exchange between electrons and ions. With preionized operation, soft x-rays are not produced on the first half-cycle for $+B_o$, but do appear for zero and negative bias fields. There is thus a striking independence of the soft x-ray and neutron signals, since the latter do not appear for $B_o = 0$. This independence also occurs in crowbarred operation in which the neutron pulse is extended while the x-ray signal is not.

A vacuum x-ray spectrometer using beryl diffraction crystals is being put into operation. It will be used for the direct measurement of the Scylla soft x-ray spectrum.

Construction of Scylla III continues and should be complete in late September.

The assumption that the Scylla ion and electron temperatures can be accounted for by adiabatic compression has been tested by means of a simple mathematical model. It is assumed that the only two processes operating are adiabatic compression and collisional interchange of energy between the ions and electrons. This model can account for the ion and electron

temperatures (1.3 kev and 240 ev, respectively) at peak compression only if the electron-ion relaxation time is greater than three times the Spitzer value.

7. In the orthogonal pinch experiment, magnetic studies of a deuterium discharge have been continued with emphasis on external field and flux measurements. Preliminary calculations of the plasma radius vs time are being made using the experimental data. Scaling of the physical dimensions and a reduction in the mirror ratio leads to larger neutron yields extending in time throughout a B_z zero. The possible causes of the events leading to the onset of field intermixing are considered to be of basic importance.

8. Electrostatic probes have been applied in the Ixion experiment to determine the radial potential distribution. The results show a region of very low electric field near the outer wall and confirm the existence of an equipotential region at the center of the device whose radius is determined by the magnetic field and the size of the end electrodes.

9. Ultra-high vacuum techniques similar to those applied in other Sherwood laboratories are being developed. Experience is being gained in the use of baked metal systems with oil diffusion pumps. With this equipment, vacua in the range of a few times 10^{-10} mm Hg are being attained.

10. A stable plasma confinement configuration called Helixion, has been proposed which reduces the cusp losses of picket fence geometries; it is adaptable to both toroidal and linear systems. Basically, it consists of a magnetic field produced by an external tight helical winding together with an open internal helix. Since the current to the latter would have to be supplied by induction in a toroidal system, the operation would be discontinuous. This drawback can be overcome by using a linear geometry, and opening up the coils of the internal helix at the ends of the tube, to provide connections to an outside source. Losses would occur at the ends, but their effect could be minimized by the use of a long tube.

A. ENTROPY TRAPPING

Work has continued using the Model III gun (LAMS-2444, p. 11) for
injection and trapping experiments in the picket fence geometry. Under
maximum output conditions (100 mm plenum pressure and 32 kv) this gun
produces a plasma jet with a mean ion energy of 10.9 kev and a number
density of 8×10^{11} ion/cm^3 measured at the input cusp of the P.F. magnet.
This plasma jet is capable of producing only a small diamagnetic signal
(typically 1 gauss), decaying with a mean lifetime of 50 µsec. The small
signal observed was apparently due to the low energy ions in the spectrum,
since increasing the base pressure in the P.F. from 4×10^{-6} mm to
3×16^{-4} mm resulted in no observable change in confinement time. Probe
measurements at the input cusp, however, did show a marked change in
behavior for different gun conditions. For example, for the 100 mm plenum
pressure case cited above $\beta < 1$ for $B > 10$ gauss, whereas for a 200 mm
plenum pressure $\beta \sim 1$ for $B < 300$ gauss and $\beta \approx 300/B$ for $B > 300$ gauss.
Similar results were obtained when helium, instead of deuterium, was
accelerated by the gun.

It has been suggested that the failure to form a sheath when a
high velocity plasma was injected into a magnetic field was due to a lack
of conduction electrons. The argument is as follows, using mks units:

$$\nabla \times \vec{B} = \mu_0 \vec{j} ,$$

so that, in cylindrical coordinates when only B_z exists,

$$\frac{\partial B_z}{\partial r} = -\mu_0 j\theta$$

5

$$j_\theta = nev_\theta.$$

The maximum value of v_θ is c, and so

$$\frac{\Delta B}{\Delta r} \approx \mu_o nec.$$

If a sheath 1 cm thick is to support a field difference of 10 kg, then the minimum electron density required is $\sim 10^{12}$ electrons/cm^3. The electron densities actually encountered in the experiments were of this order of magnitude.

Using this requirement of the minimum electron density and making some reasonable assumptions, it is possible to estimate the field strength and the minimum total amount of plasma required as a function of the kinetic energy of the injected ions. For example, for a 3 cm radius plasma jet (and 1 cm sheath), having a mean deuteron energy of 500 ev and delivered in a 2 µsec pulse, it appears that a plasma jet energy of about 10 joules would be required to displace a 1200 gauss field. This is in good agreement with experimental measurements.

The foregoing discussion pointed up the need for increased plasma density in order to trap the desired high β plasmas at higher magnetic fields. The simplest way to increase the density was to move the gun as close as possible to the input cusp; the total amount of plasma reaching this cusp was thereby increased by a factor of ten. Also, the length of the plasma blob was reduced by operating the gun with higher plenum pressures which produced lower average ion velocities.

Under these conditions it was found possible to produce a $\beta = 1$ region in the input cusp at fields up to 2000 gauss. A probe at the entrance cusp indicated a $\beta \approx 1$ open time of 3 µsec. In the midplane of the P.F. a $\beta \approx 1$ region was found to develop rapidly and then decay with a mean lifetime of approximately 30 µsec. The development time of this region furnishes a crude time of flight measurement of the energy of the

particle being trapped and indicates that 100 to 500 ev deuterons are responsible for the main diamagnetic signal. In addition to the simple diamagnetic effects expected, motion of the high β region was studied by correlating simultaneous measurements of magnetic perturbations at several locations (two probes 90° apart on the ring cusp and one probe located on the axial cusp). A slow ($\sim$ 10 μsec period) breathing (radial oscillation) motion was observed and also a smaller amplitude "sloshing" motion of the entire plasma ball.

Further magnetic probe studies were made in an effort to determine the dimensions of the trapped plasma. From the measurements it was found that to be certain of producing a $\beta = 1$ region in the center of the magnet it was necessary to reduce the cusp field considerably from the maximum field which could be penetrated in a high β plasma. Fig. 1 shows a plot of the results at 300-gauss cusp field. From this is seen that (a) the plasma does not have the expected biconical shape (half angle between 45 and 60°), but is relatively long and narrow; (b) the sheath is several cm thick, and (c) the plasma is uncomfortably close to the walls of the vacuum vessel.

In order to minimize any interaction of the plasma with the walls a much larger apparatus has been designed. This takes the form of a calked picket fence (uniform magnetic field plus a single turn coil with the currents arranged so that there is a zero in the field at the center of the system) having a vacuum chamber 5 ft in diameter and 10 ft long.

B. PLASMA GUN DIAGNOSTICS

A procedure has been developed for making direct measurements of the electric field in the plasma sheath in the coaxial gun. Initially, such measurements were made with a voltage divider placed between the gun electrodes as shown in Fig. 2. When the current sheet is advancing toward the probe, (position 1) there is negligible magnetic flux crossing the probe position, and so the measured voltage is due entirely to noninductive
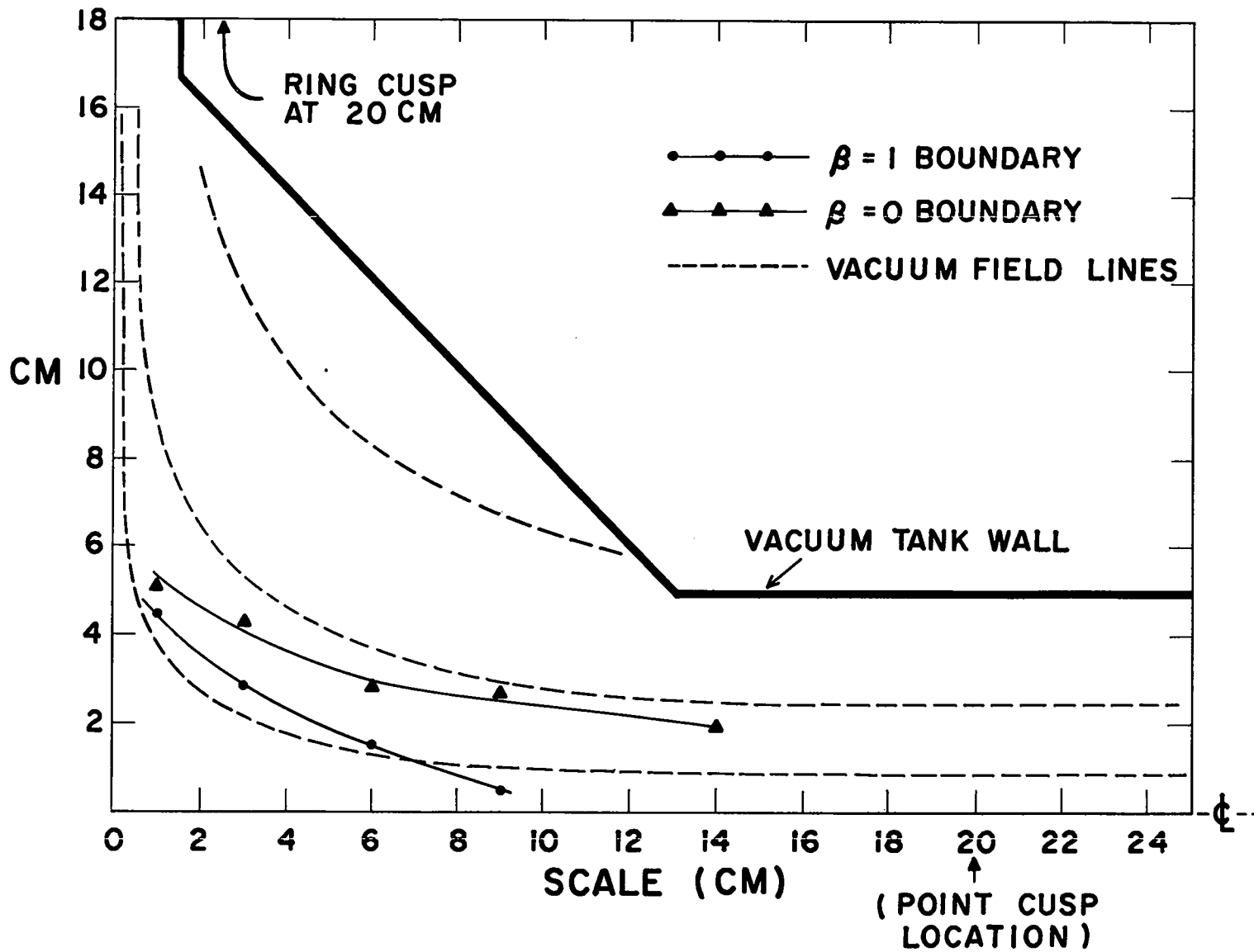
Fig. 1. Shape of plasma (one quadrant) in 300-gauss point cusp field
17 μsec after gun firing (origin 67 cm from gun).
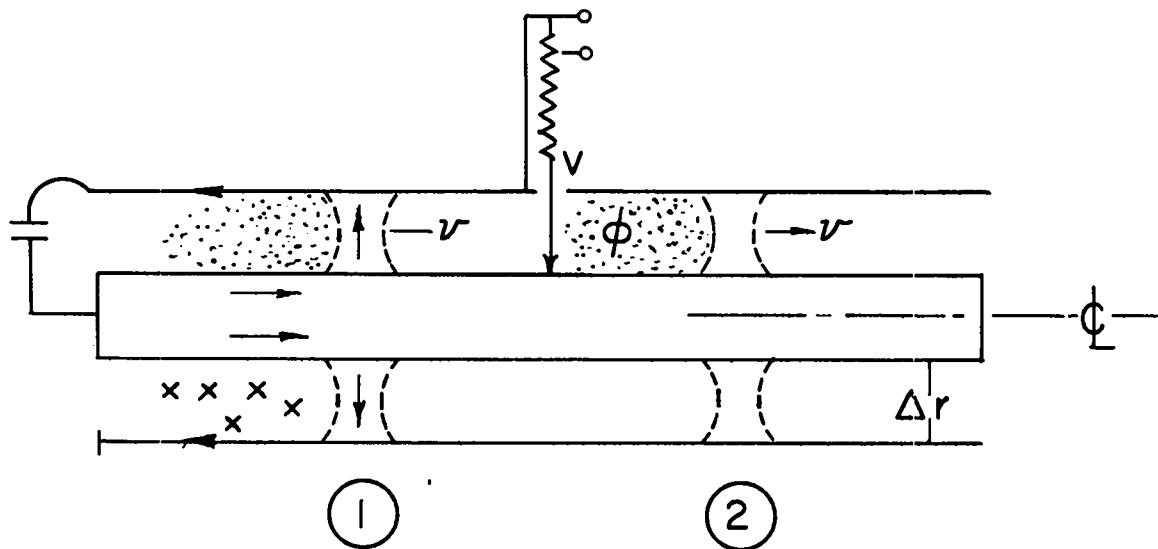Plasma source on left.

Fig. 2.   Measurement of electric field with voltage
          divider between gun electrodes.

terms, e.g., IR drop and possible electrode sheath drops. Hence, in general,

$$V = V_s + IR + \frac{\partial \theta}{\partial t} \quad ,$$

where V_s accounts for electrode sheath drops, and θ is the total B_θ flux on the right of the probe in Fig. 2. In position one, $\partial \theta / \partial t$ is negligible, but as the current layer crosses the probe, this term becomes predominant, and is approximately

$$\frac{\partial \theta}{\partial t} = B_\theta \cdot v \, \Delta r. \tag{1}$$

Measurements under standard operating conditions show that $V_s + IR$ is about 100 volts prior to sheath arrival, and that $\partial \theta / \partial t$ is 700 to 800 volts when the current layer passes. If B_c is also measured, equation (1) permits a determination of velocity; for the measured cases, this figure agrees well with two-point velocity measurements.

If the $V_s + IR$ term were primarily resistive, a plasma temperature of less than 3 ev would be implied. In order to determine which effect produces the voltage drop in the frame of the moving plasma, differential voltage probe observations were made. Measurements of the electric field in the plasma as a function of radius demonstrated clearly that approximately the entire $V_s + IR$ term is due to a thin cathode sheath at the center electrode. At any position farther than 3 mm from the cathode, the measured E field is quite accurately equal to $|\vec{v} \times \vec{B}|$. The substitution of helium for deuterium in the gun approximately doubled the cathode sheath drop, indicating that this system is acting quite like a classical glow discharge.

C. SKEW TRAPPING

A modification of the ion gun has been completed allowing much more detailed measurements to be made on the trajectories of the beam in the magnetic field. These modifications consist of (a) magnetic shielding of the beam in the accelerator tube and (b) mounting the gun in a cradle so that it could be accurately positioned. The magnetic shielding of the

gun was accomplished by fabricating the lens system from iron tubing, and by adding an iron collimator tube to the assembly up to the entrance to the magnet vacuum chamber. The positioning device consists of a mount for the gun which may be displaced from the center line of the magnet, and a sliding vacuum seal where the collimator enters the vacuum chamber.

Studies of the trajectory of the beam during its first transit have been carried out using a movable plate, placed perpendicular to the axis of the magnetic field, and covered with a scintillating material to indicate the position of the beam impinging on the plate. By observing the displacement of the beam spot as the plate is displaced a known amount along the axis, it is possible to determine the ratio of momentum perpendicular to and parallel to the magnetic field. The results of these measurements, made at the point cusp farthest from the injector, for the symmetric magnetic field conditions are shown in Fig. 3, and for asymmetric field configuration in Fig. 4. The results indicate that it is quite easy to reflect the beam back into the confinement region from the far mirror; this is of some interest regardless of whether confinement for long times is possible or not.

Some attempt was made with the same technique, to determine subsequent orbits in the line cusp region. It was found that the beam, or at least parts of the beam, made up to five reflections on the line cusp before becoming too faint to be seen. However, this technique is not too satisfactory for determining subsequent orbits. A small scintillator probe attached to a photomultiplier was utilized to investigate the possibility of confinement under conditions where the probe was small enough not to seriously disturb the system. However, no clear evidence for such confinement was obtained.

A possibility exists for losses other than at the cusps. If the corners of the vacuum chamber extend too far into the containment region, the particles strike them as they follow lines of force from the point cusp up into the line cusp region and so are lost. When these corners

11

IO KG MAX PICKET FENCE FIELD
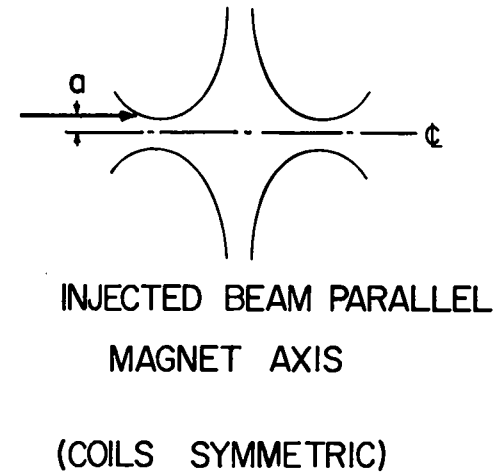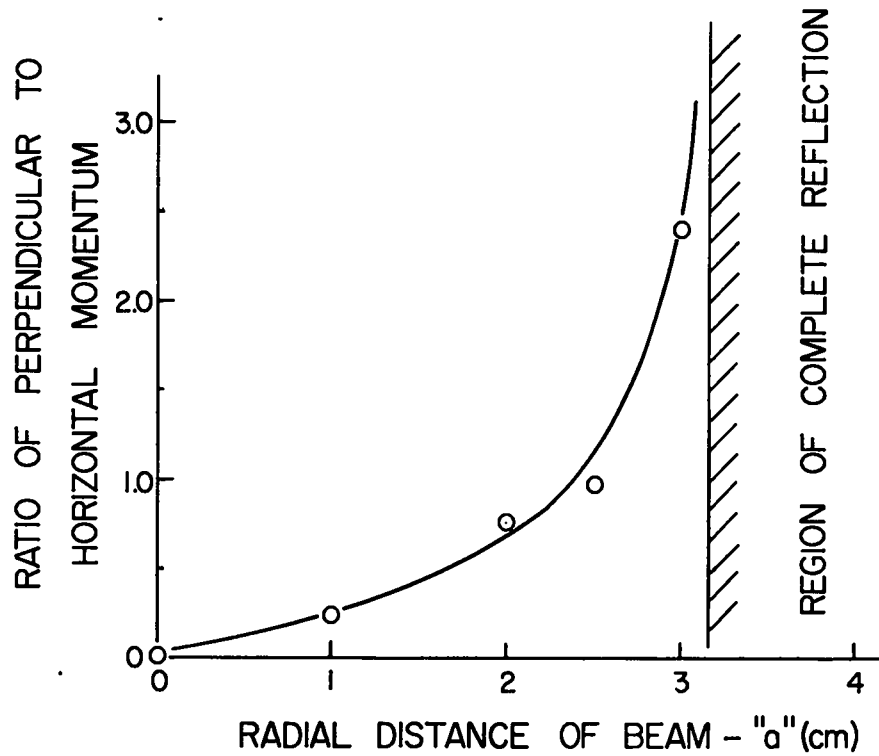## 30 KEV H⁺ BEAM

Fig. 3. Movement of momentum (perpendicular to horizontal)
ratio in symmetric magnetic field.

IO KG MAX PICKET FENCE FIELD
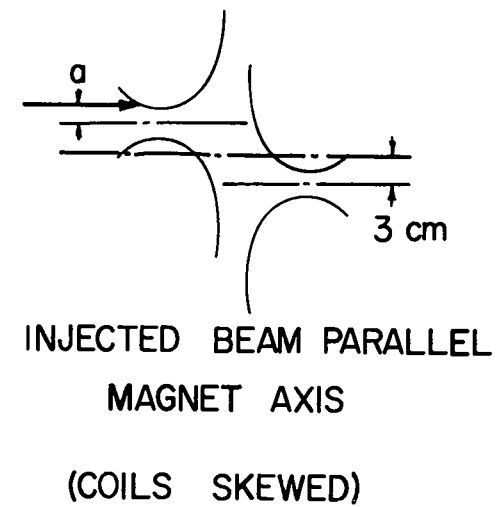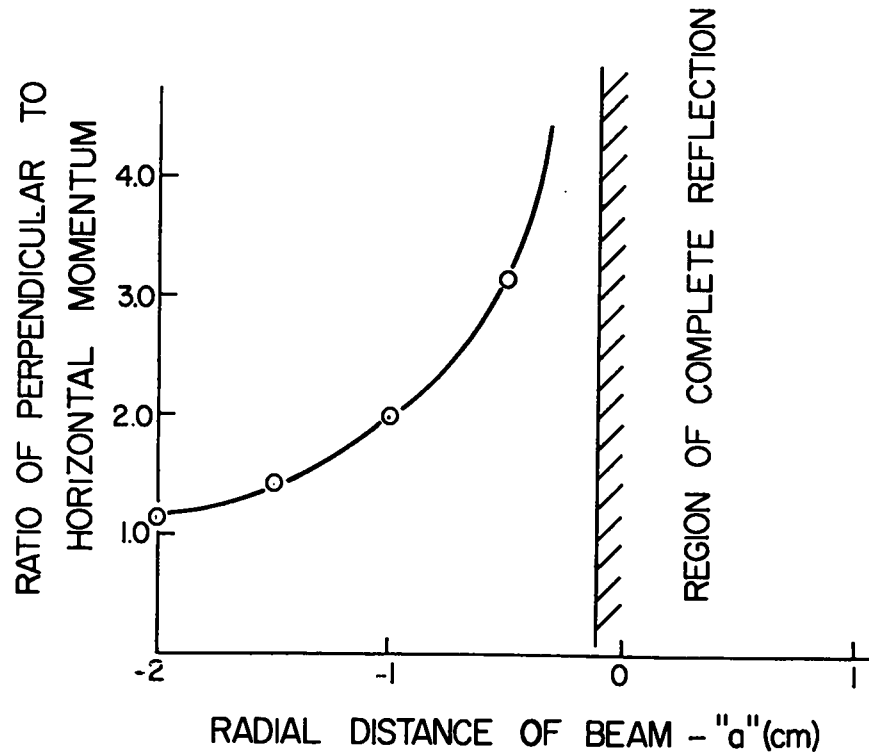## 30 KEV H$^+$ BEAM

Fig. 4. Movement of momentum (perpendicular to horizontal)
ratio in skewed magnetic field.

were painted with a scintillator, the four or five spots corresponding
to the transits of the beam previously determined were all observed. It
can be concluded, therefore, that on each transit an appreciable fraction of
the beam was being scraped off on the vacuum chamber wall. Attempts are
being made to eliminate or reduce this loss channel by decreasing the
radius of curvature of the particles.

D. SCYLLA

X-RAY DIAGNOSTICS

Introduction

The previously reported analysis of the spectrum of soft x-rays
emitted from the Scylla discharge has shown that the electron temperature
reaches about 240 ev at the peak compression of the second half-cycle.
This result has been obtained only by averaging over several hundred
discharges, and special interest therefore attaches to a procedure which
permits the electron temperature time history to be followed throughout a
single discharge, as well as yielding the electron temperature at peak
compression. Such information is desirable when studying the effect of
variable parameters on the electron temperature, in estimating the rate
of energy partition between ions and electrons, and the rate of loss of
particles through magnetic mirrors, and the effect of preionization upon
subsequent discharge characteristics.

Method

If the electron velocity distribution is assumed to be Maxwellian,
only two points on an absorption curve are sufficient to determine the
electron temperature. The functional dependence of the two-point
absorption curve is independent, to a good approximation, of the source
density and impurity concentration. A double x-ray detector, consisting
of two complete pinhole-absorber and scintillator-photomultiplier assemblies,
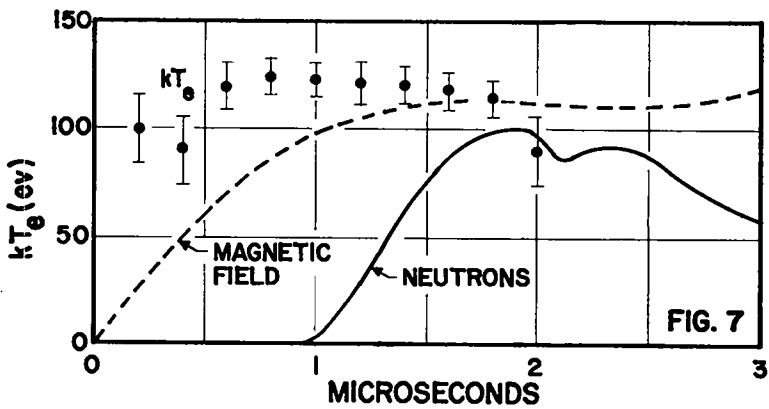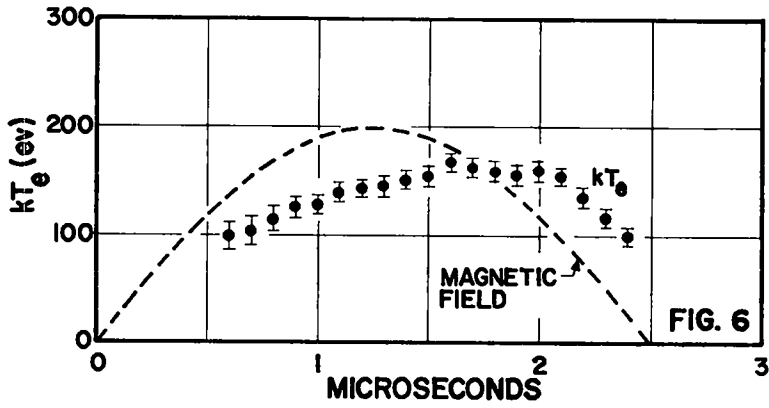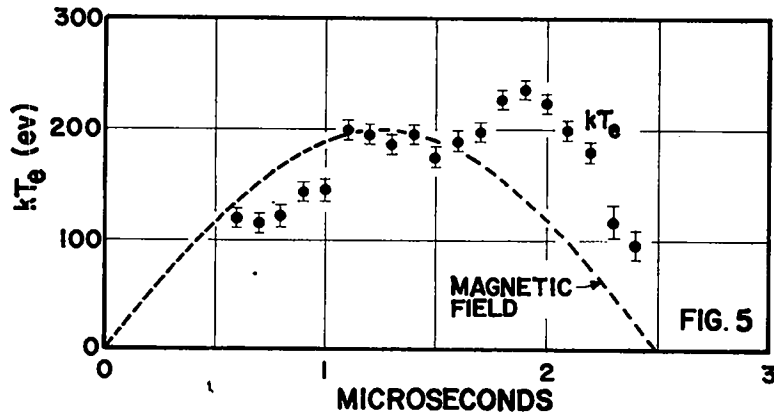has been tested and calibrated for axial viewing of the Scylla discharge.

The electron temperature, as a function of time, is obtained by comparing the ratio of the photomultiplier signatures with the calculated dependence of the transmission ratio on temperature.

Results

Figs. 5 and 6 show results for two successive Scylla G (or I) discharges, where the curves refer to the second half-cycle of the discharge current. In both cases the maximum kT_e is reached about 0.5 μsec later than the peak of the magnetic field, in qualitative agreement with the hypothesis that the electrons gain energy from the higher temperature deuterons as well as from the adiabatic compression. The irregular features of Fig. 5 show that additional processes are necessary for a complete explanation of the temperature histories. Fig. 7 is for a first half-cycle, power-crowbarred discharge, with axial pinch preionization and reverse, externally-applied quasi-static B_0, so that neutron production occurs on the first half-cycle of current. Under these conditions, kT_e is always lower than with usual Scylla G operation, and displays a rather flat characteristic. As is seen in Fig. 7, the neutron production continues after the electrom temperature has become too low to be recorded by the present technique. There is no question that these experimental data are in disagreement with any theoretical adiabatic model based on a constant total number of particles with no radiation loss.

Measurements have been made of the soft x-ray emission and electron temperature for first and second half-cycle 100-kv operation with axial pinch preionization as a function of the direction of the externally applied quasi-static B_0. The results are summarized in the following table:

| B_0 | First Half-Cycle | | Second Half-Cycle | |
	kT_e(ev)	Neutrons	kT_e(ev)	Neutrons
+ 2 kg	no x-rays	none	147	good
0 kg	138	poor	175	good
- 2 kg	107	good	108	good

Figs. 5,6,7.   Measurements in Scylla discharge (Figs. 5 and 6 are for
              successive second half-cycle discharges; Fig. 7 is for a
              first-half-cycle, power-crowbarred discharge.)

The data show that axial pinch pre-excitation generally results in lower kT_e than is obtained in the second half-cycle with ordinary low-power rf preionization, presumably because of the greater contamination. Furthermore, the absence of soft x-rays on the first half-cycle with aiding B_O must be taken as an indication of low kT_e rather than the absence of contamination, since contamination occurs with both zero and reverse B_O and pinch preionization. These observations are in agreement with the previous result that adding B_O does not lead to an imploding sheath with subsequent neutron emission.

VACUUM X-RAY SPECTROMETER

A vacuum spectrometer has been constructed with the object of providing a flexible instrument in which the table holding the dispersive element and that holding the detector arm can be independently rotated and set with high precision. It will be used in the vacuum ultraviolet for the Zeeman experiment (LAMS-2444, p.34) and also as an x-ray diffractometer for measuring soft x-rays from Scylla.

Fig. 8 shows the instrument with a soft x-ray tube of LASL design at the left and a proportional counter at the right on its detector arm. Adjustment of the rotational motions is made by two identical 11-in. Moore rotary tables adjustable to 5 sec of arc. The side ports of the vacuum chamber are so positioned that all deflection angles between zero and 165° can be covered by indexing the chamber, with fine angular adjustment being provided by the flexibility of the two sylphon bellows.

Alignment and resolution tests have been performed with beryl single-crystal plates oriented on the $10\underline{1}0$ plane (d = 7.96 KXU), polished to have natural diffraction widths corresponding to 20 and 40 sec of arc. A crystal of broader resolution ($\sim$ 200 sec) is being prepared. The crystal has been tested using $CuK\alpha_1\alpha_2$, $AgL\alpha_1\alpha_2$, $AlK\alpha_1\alpha_2$, and $CuL\alpha_1\alpha_2\beta_1$ characteristic radiations. For application to the Scylla continuum over the extended source, collimation will be by means of soller slits in the source and detector arms. These consist of stacked 5-mil foils spaced by 0.020 in. with a collimated area 1 in. square.
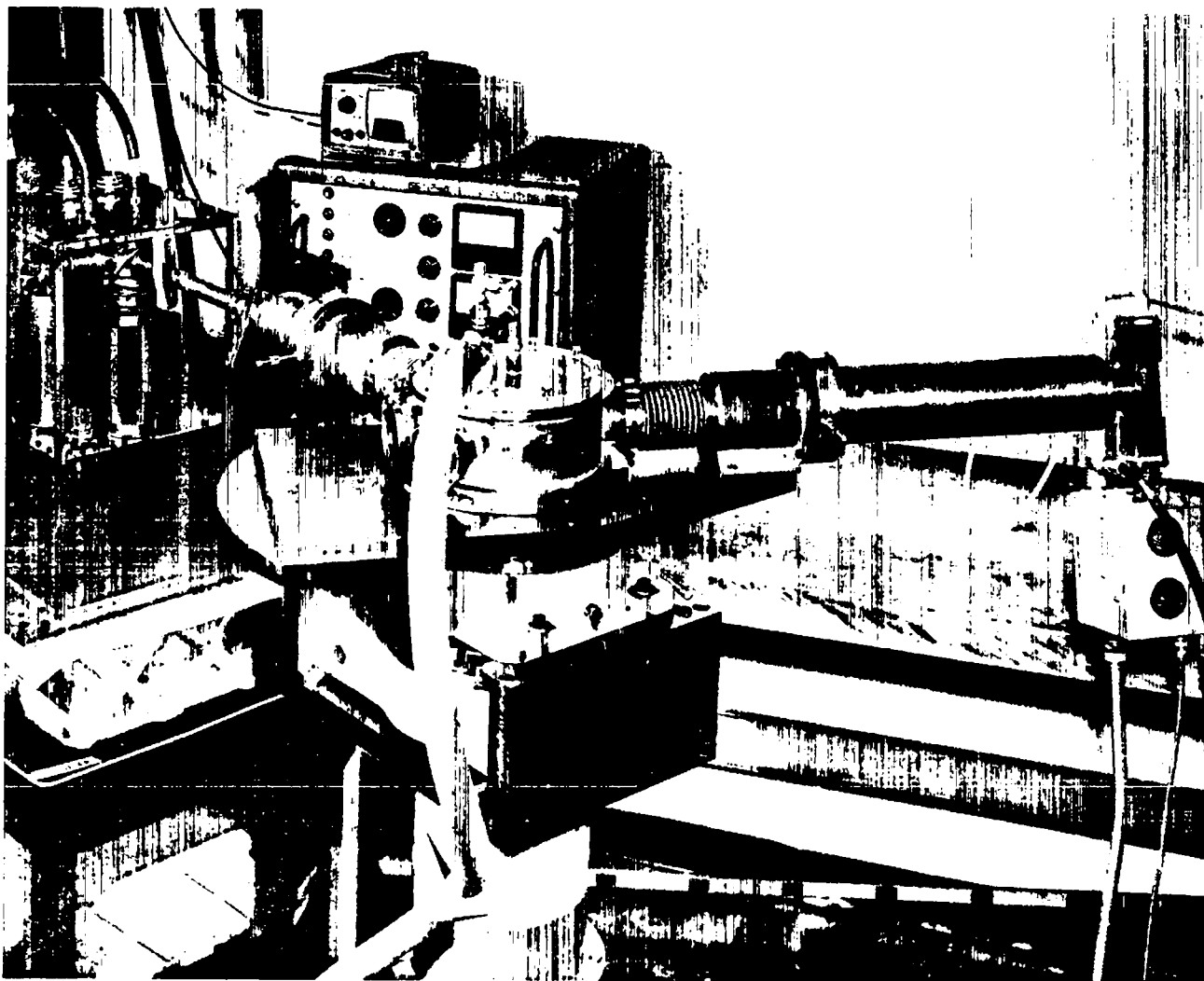
17

Fig. 8.   Vacuum spectrometer for Scylla x-ray measurements

SCYLLA III

The design of the new version of the Scylla machine which was
described in LAMS-2444 (p. 31) has been completed. The construction
phase of Scylla III is well underway with a projected completion date in
late September.

The device in its present state is shown in Fig. 9; the 120-kj,
100-kv capacitor bank is seen on its platform with the top part of the
Marx generator in the background. The 5-stage Marx generator will be used
to charge the 100-kv bank. The vacant areas in the 100-kv bank are
reserved for additional energy storage capacitors as previously described.
The 100-kv capacitor bank is located above the Scylla machine with special
RG-19-14/U cable connecting the bank to the parallel plate transmission
lines leading to the single-turn Scylla coil. The special cable consists
of an inner-conductor of copper braid normally used as RG-14A/U and an
outer-conductor of RG-19A/U outer-conductor braid. Such cable has an
inductance of 0.04 μh/ft.

TEST OF THE ADIABATIC-COMPRESSION, TEMPERATURE-RELAXATION MODEL OF SCYLLA OPERATION

The model under investigation is assumed to describe Scylla operation
following the initial ionization and heating phase. It shows the temperature
development of the ions and electrons in a fully ionized plasma as a
consequence of an adiabatic compression exerted by the increasing magnetic
field, with simultaneous relaxation of the ion and electron temperatures,
as given by the Spitzer energy exchange time for two Maxwellian distributions.
All particle and radiation losses are ignored.

The present approach is based on an analytic solution of the
differential equations, designed as a check on the numerical result and
at the same time serving to display the effect of varying the parameters
of interest, i.e., the relaxation time and the γ of the adiabatic law. The
energy-transfer relaxation time calculation of Spitzer assumes that the
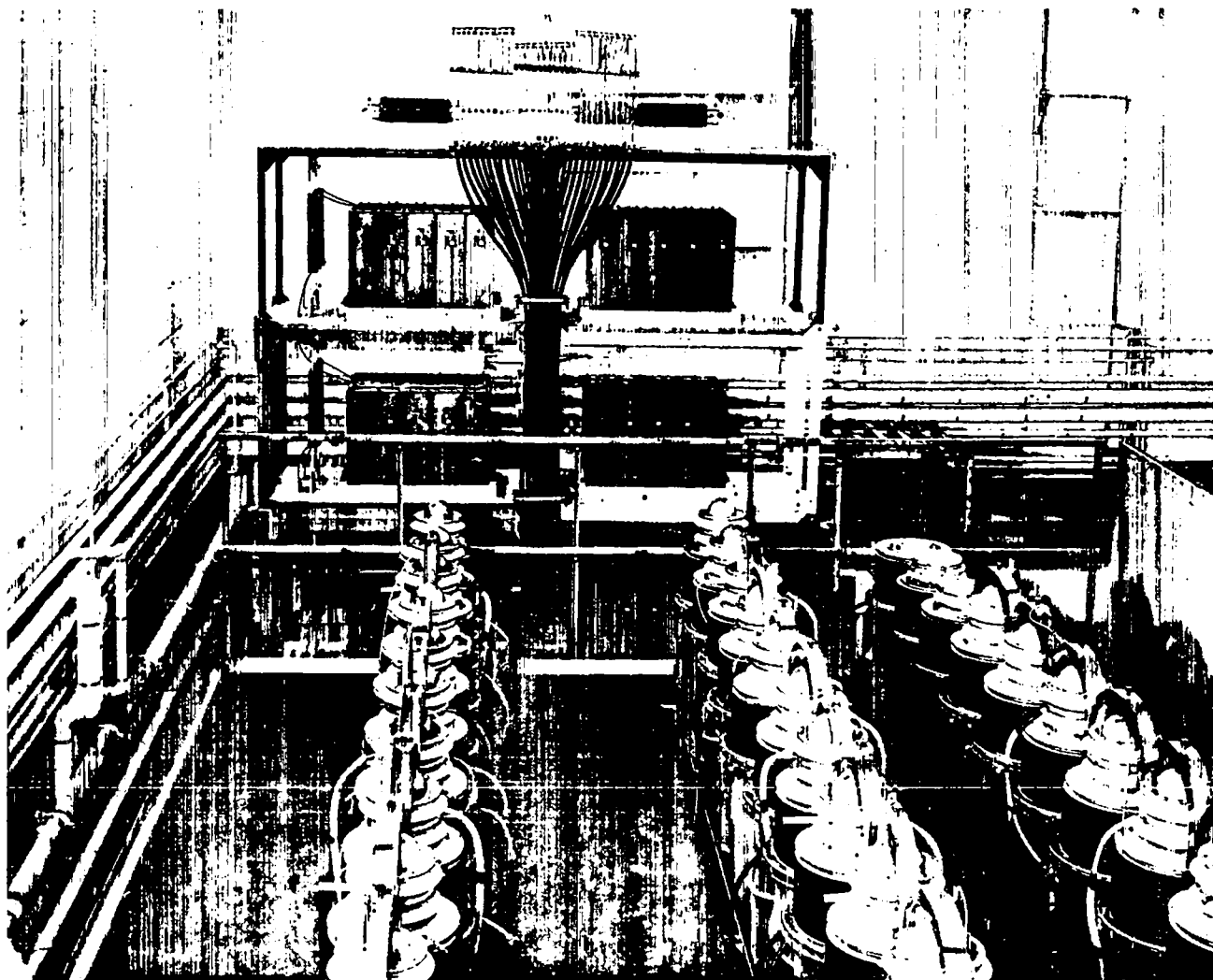
Fig. 9. Present status of Scylla III

interacting species can be described by Maxwellian distributions throughout the relaxation process. This leads to an underestimate of the relaxation time, especially for a large temperature difference. A more detailed calculation, based on transport equations for the interacting species with a Fokker-Planck collision term, bears out the qualitative expectation that most of the contribution to the energy exchange rate from ions to electrons comes from the low velocity part of the electron distribution function with attendant depletion of low-velocity electrons. The corresponding relaxation time exceeds Spitzer's equilibrium value by factors of order 1.5 to 2.

The accompanying graph (Fig. 10) shows plots of ion and electron temperatures, T_D and T_e, as functions of time as given by the analytic solutions. The values of the temperatures at peak magnetic field time t_o = 1.25 μsec were assumed to be T_D = 1.3 kev, T_e = 240 ev, and the number densities n = 5 x 10^{16} cm^{-3}. Curves are drawn for γ = 5/3, with relaxation time τ as parameter. Values of τ were chosen to be $\rho\tau_s$, where τ_s is the Spitzer relaxation time and ρ was taken to be 1, 2, and 3. It is seen that the computed curves of T_e and T_D reproduce the observed temperatures reasonably well for ρ > 3, i.e., when the electron-ion relaxation time is taken to be greater than three times the Spitzer value.

ORTHOGONAL PINCH

Decreasing the mirror ratio (R_m) to 1.02:1 increases the neutron yield to 6 to 8 x 10^6 n/discharge. The extended neutron pulse shown in Fig. 11 (sweep speed 2 μsec) is more typical as $R_m \rightarrow$ 1. For R_m < 1, neutron yield decreases by a factor of 8 to 10 for almost identical geometry and field parameters. Magnetic probes record very small reversed fields of 0.1 μsec duration in this case.
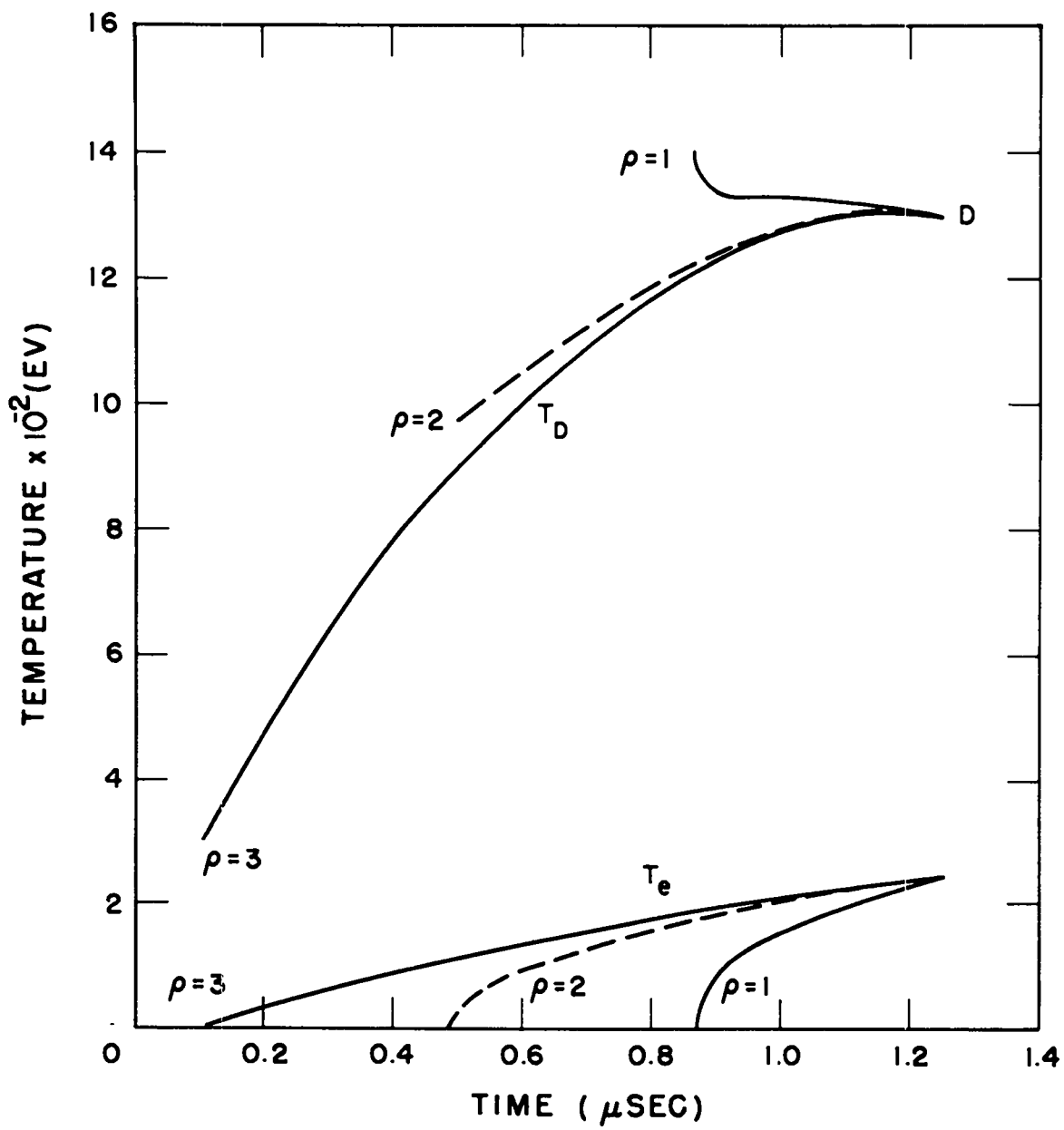
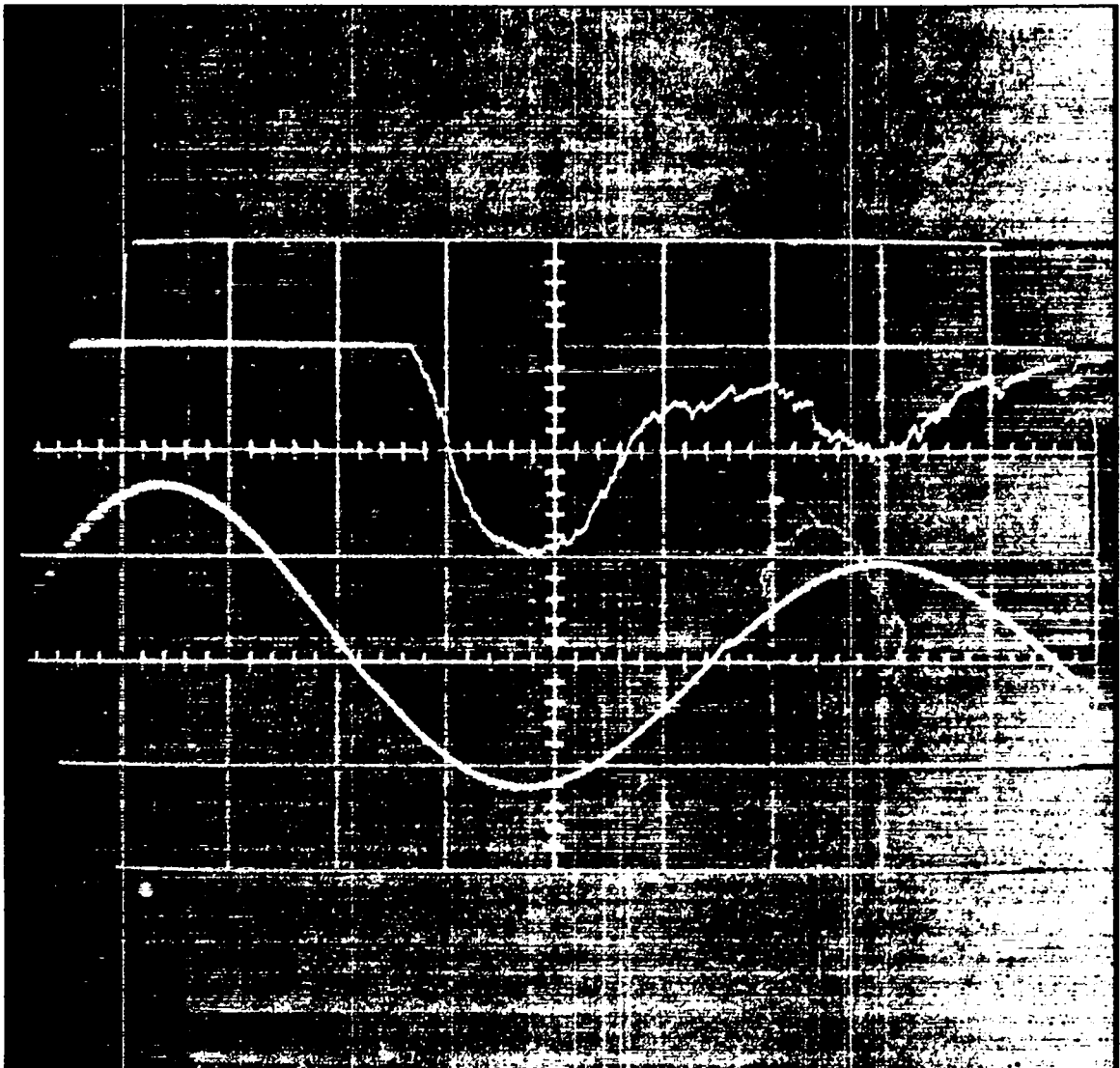Fig. 10. Ion and electron temperatures as function of time

Fig. 11. Neutron pulse in orthogonal pinch. Upper trace
          shows neutron emission as function of time;
          lower trace is machine frequency.

Perturbation of the plasma due to a finite feedpoint separation has been investigated by collapsing thin wall metal tubes in the vacuum magnetic field. By reducing the separation to about 1/4 mm, i.e., 1 part in 10^3 of the inner coil surface, the asymmetry becomes negligible. Separation of 1.5 mm in 100 mm produced an asymmetry of roughly 5 mm.

The mechanisms responsible for neutron production are far from understood; however, a simple calculation shows that field intermixing is the most likely means whereby the plasma is heated. A preliminary calculation of the plasma radius vs time, on the basis of the experimental measurements, offers the possibility of distinguishing between an adiabatic and a field intermixing heating process. The increased neutron yield as $R_m \rightarrow 1$ can be explained by a dilution of the confined plasma caused by increased end losses (plasma streaming). In this case, plasma energy obtained from the magnetic field is shared by the fewer remaining particles. Confinement of the plasma from the walls while $B_z = 0$, i.e., between the second and third half cycles, is provided by a secondary current sheath which turns out to be inertial.

The cause of the onset of field intermixing is of basic significance. Processes involving the nonlinearity of $E\sigma$ at high current densities and the runaway of large numbers of electrons at radial positions where $Bz = 0$ result from situations involving trapped reversed magnetic fields. In the latter process, unstable plasma oscillations (two stream instability) may develop which are capable of carrying charged particles across magnetic field lines.

E. PERHAPSATRON S-5-ZEUS

The high energy modification of Perhapsatron S-5 was put into operation and preliminary data were obtained before a crack opened in the quartz vacuum vessel which necessitated replacing the quartz vessel. Table I lists the different energy supplies and the firing sequence of the several components.

TABLE I

	Energy Supply	Firing Time
Iron bias*	0-20 kv 700 μf (5 μsec rise) I (per iron core) ~ 1.5 ka	0 sec
Iron bias crowbar	(8 μsec decay)	7 μsec
B_z magnetic field	0-3 kv (0-9000 gauss) 0.058 f (13.6 μsec period)	2.4 μsec
Preionization	0-20 kv 7.5 μf (13 μsec period) I_{max} ~ 10 ka	~ 10 μsec before B_θ supply.
Main Discharge, B_θ	0-20 kv 5600 μf (~ 130 μsec period) (four feed points)	4.8 μsec

*The iron bias supply is isolated from the B_θ voltage by 2.2 mh inductances. It is fired prior to the B_z supply as it was found that with a B_z magnetic field the gas broke down when the iron bias voltage was applied.

Figs. 12 and 13 show the discharge currents obtained with variation of B_θ stabilizing field. The behavior agrees approximately with calculations and a peak current of 870 kiloamp was obtained at 20 kv.

Preliminary measurements of the neutron yield showed an approximately linear increase with current and voltage up to 17.5 kv. Tests at higher voltages were terminated by the failure of the quartz torus. Neutron bursts of approximately 10^8 per discharge have been obtained.
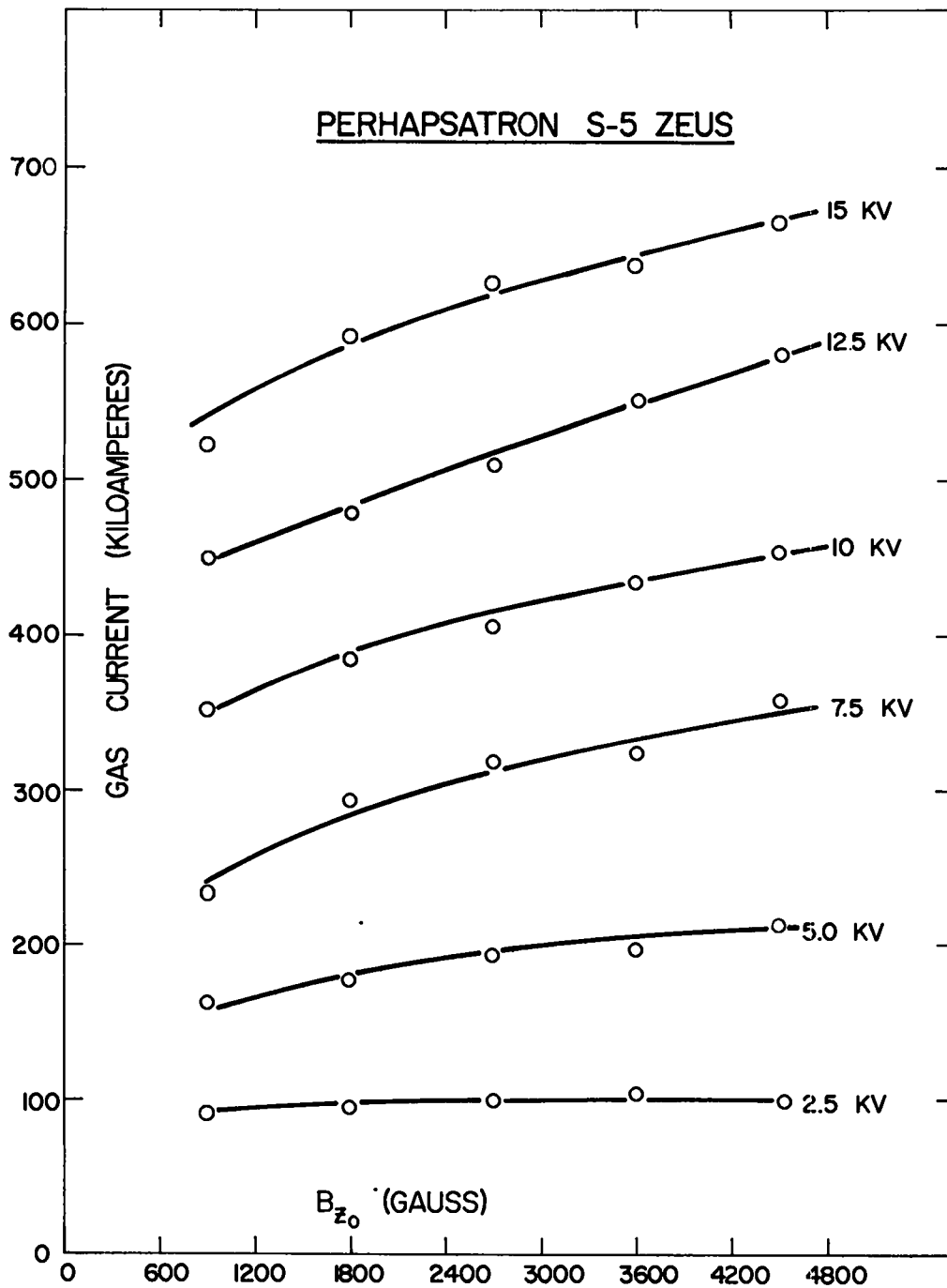
PERHAPSATRON S-5 ZEUS

Fig. 12. Discharge current in Perhapsatron S-5-Zeus as
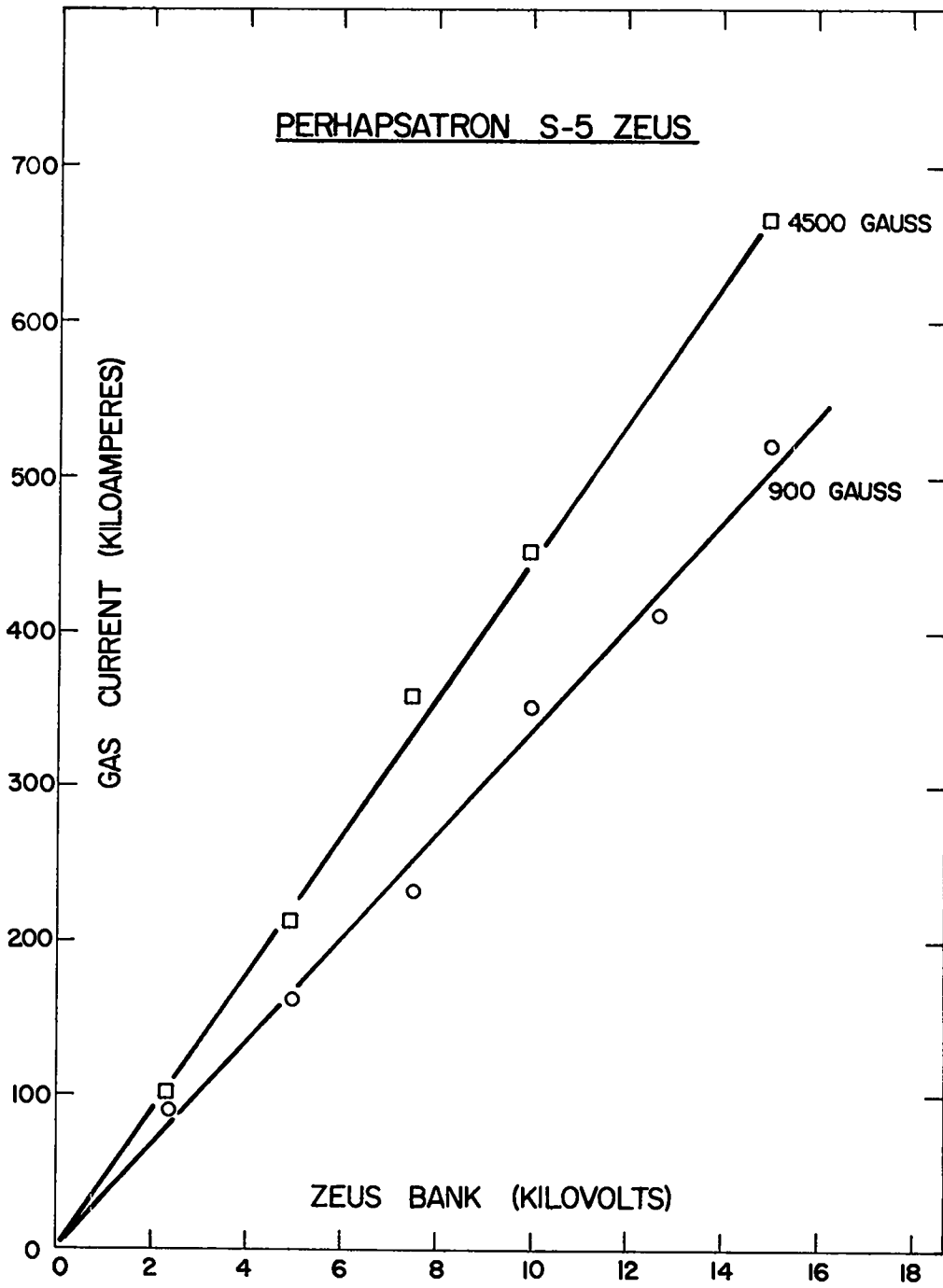function of B_θ for various bank voltages.

26

Fig. 13. Discharge current in Perhapsatron S-5-Zeus as
function of bank voltages for two values of B_z.

F. IXION

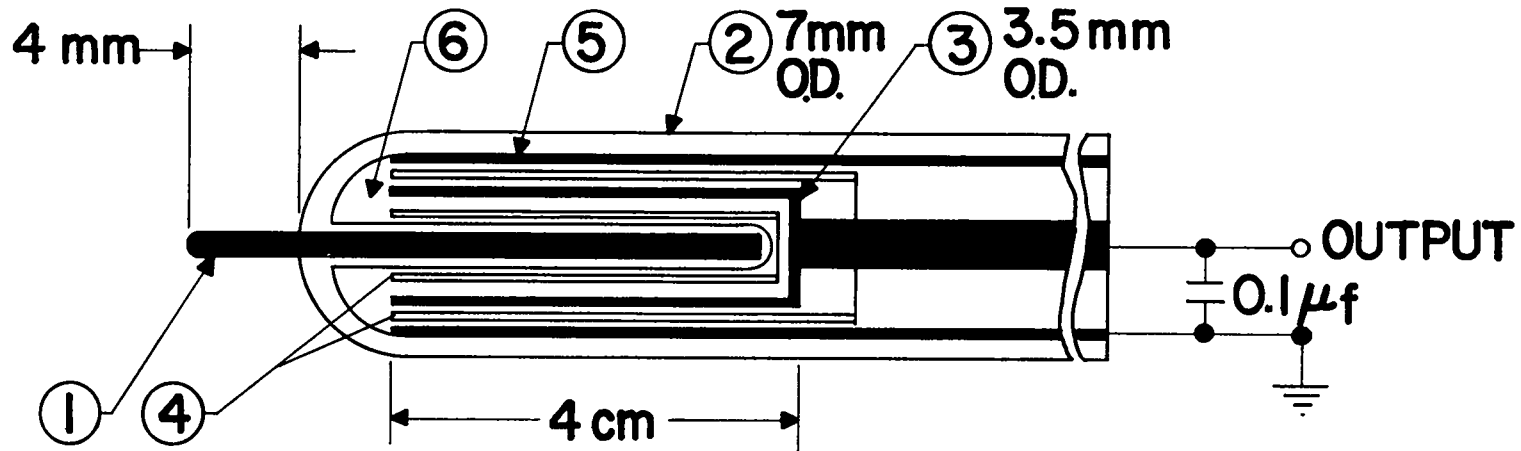## ELECTROSTATIC PROBE MEASUREMENTS

General

Measurements of potential distributions in Ixion have been made using a capacitively coupled, high-impedance electrostatic probe. The basic construction of the probe is shown in Fig. 14. The voltage signal is picked up by direct plasma contact with a tungsten wire sealed through the end of a 7 mm diameter Pyrex tube. The pickup electrode is capacitively coupled through an oil-filled cup to a grounded 0.1- μf, glassmike capacitor. The voltage across the latter is measured with an oscilloscope, the setup being essentially a capacitor divider. Considerable care must be taken in the design of the low capacitance coupling portion of the electrostatic probe described here. The oil dielectric was the only suitable one of those tried (Pyrex, quartz, Teflon, ceramic).

Potential Distribution During Rotation

The potential distributions 100 μsec after the beginning of the Ixion current as deduced from probe signals are shown in Fig. 15. The data are for the central plane and also for a plane 18 cm to the north. The solid points represent values obtained with probe positins which do not observably disturb the Ixion rotation. The remainder of the points were secured under probe-induced, semi-breakdown conditions. These are given only for completeness and show that the probe does indeed see a larger per cent of the voltage change as it is inserted deep into the active portion of the discharge. For comparison, a logarithmic potential curve is shown assuming an effective center rod of 4.5 cm radius as predicted from the measured vacuum magnetic field, assuming that flux surfaces are also equipotentials.

These data show the following points of interest:

1) The potential near the walls is lower than that corresponding to a logarithmic variation with radius. This voltage suppression near the

4 mm

⑥ ⑤ ②7mm O.D. ③ 3.5mm O.D.

OUTPUT

0.1 μf

① ④

4 cm

1.- TUNGSTEN ELECTRODE.
2.- PYREX ENVELOPE.
3.- ELECTROSTATICALLY COUPLED CUP.
4.- INSULATING SPACERS.
5.- STAINLESS STEEL ELECTROSTATIC FIELD.
6.- MARCOL OIL FILTER.

Fig. 14. Electrostatic Probe

IXION VOLTAGE PROFILE
FROM ELECTROSTATIC PROBE
IOO MICRO-SECONDS AFTER CURRENT
ONSET.

OPEN SYMBOLS = DATA POINTS
WHERE PROBE CAUSED
PERTURBATION.

SOLID SYMBOLS = DATA POINTS
WHERE PROBE CAUSED NO
PERTURBATION.

UNPERTURBED IXION VOLTAGE
= 4.8 KV

VACUUM
POTENTIAL V

■ } MID PLANE PIVOTED
□ } PROBE

● } MID PLANE SIDE
○ } PROBE

▲ } NORTH SIDE PORT
△ } PROBE

$$V = \frac{LOG \frac{r}{4.5}}{LOG \frac{12}{4.5}}$$
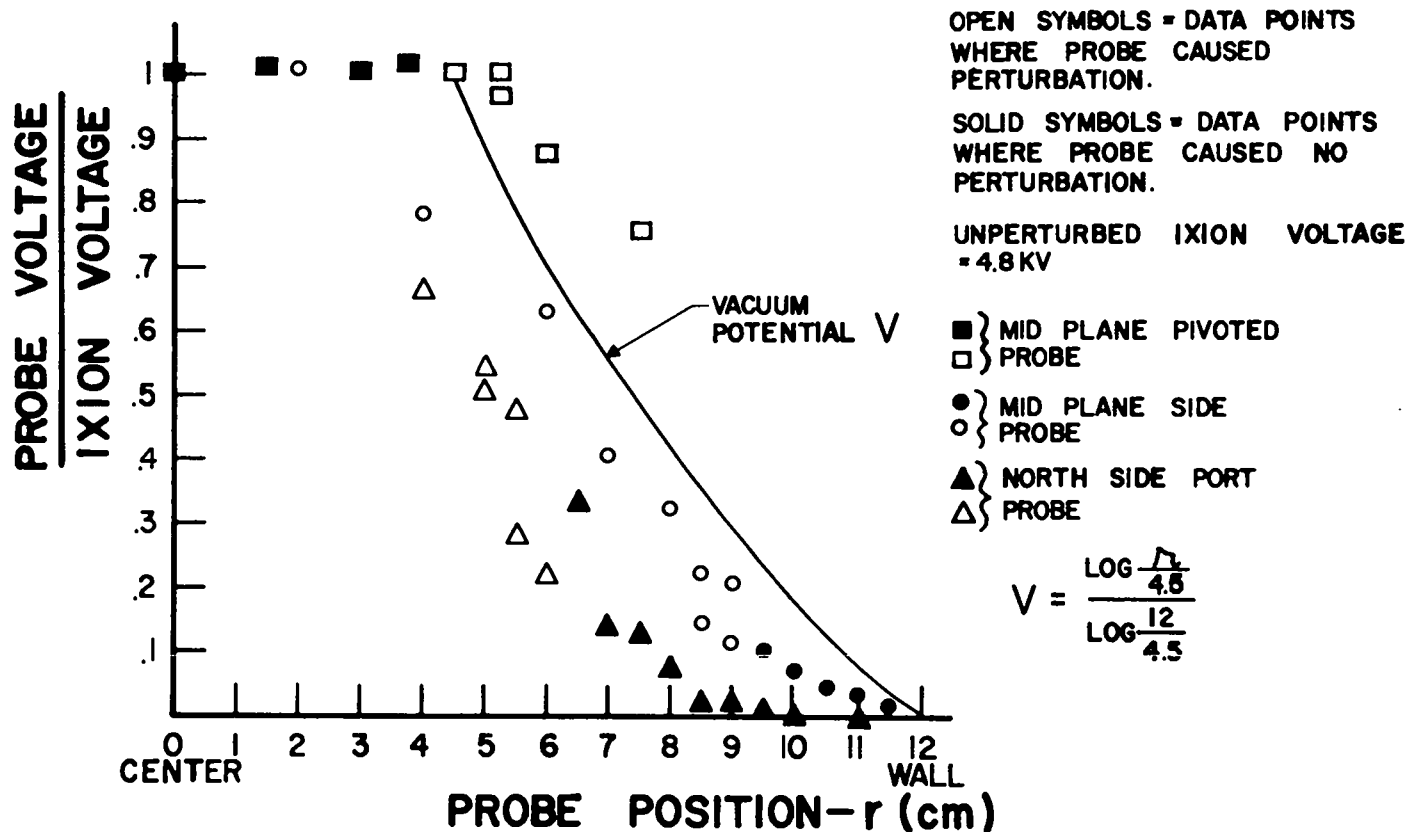
PROBE POSITION—r (cm)

30

Fig. 15.   Potential distributions in Ixion as derived from probe signals.

walls may result from lowered resistance produced by the influx of wall impurities (ion and/or neutrals).

2) Although it is not possible to probe adequately in the neighborhood of a 5 cm radius without seriously affecting the discharge, the indications are that the effective center rod is near the 4.5 cm radius that would be predicted, assuming that magnetic flux surfaces are equipotential surfaces.

G. SCATTERING OF MICROWAVES BY AN IONIZED GAS

The object of this experiment is to measure the intensity, frequency spectrum, and angular distribution of microwaves scattered incoherently by the collective oscillations in an ionized gas (LAMS-2444, p. 52). It was previously reported that the noise and spurious oscillation spectrum of the high power 10 cm-CW magnetron being used as the primary source of radiation completely masked the presence of any scattered radiation. Stabilization of the magnetron power supply failed to improve this situation, and it was found necessary to employ high and low pass microwave filters with a total power rejection ratio between pass band and wings of 150 db. With these filters properly disposed in the transmission and detection circuits (low pass in the transmitter line, high pass in the detection line) it is now possible to beam 200 watts into the scattering chamber and still detect changes in the black body radiation which is characteristic of small temperature changes in the microwave absorber surrounding the chamber.

To measure electron density in the scattering chamber a CW 10,000 mgc/sec phase shift interferometer fed by a low power klystron has been constructed. Its present sensitivity lies somewhere between 5×10^8 and 10^9 electrons per cm^3. To attain long time stability a Pound frequency stabilizer was built for the klystron power source and has been operated successfully. Measurements on the plasma contained in the scattering chamber show that the electron density created in discharges so far is too low for

the scattered signal frequency to fall within the pass band of the receiver. For this reason steps are being taken to improve the efficiency of the r.f. ionization system.

H. CALCULATION OF IONIZATION AND EXCITATION PROBABILITIES IN A PLASMA

Studies are being directed toward the calculation of the probability of ionization and excitation of impurity atoms by electron collisions in a plasma. Such calculations all depend ultimately upon the numerical evaluation of the Coulomb interaction integrals for the radial part of hydrogen-like wave functions. These have been completely integrated in terms of hypergeometric functions of two and three variables. The known series representations for the functions all converge only for a limited range of values of variables, and unfortunately, for most of the calculations involved here the variables lie outside this region of convergence. Attempts are being made to develop suitable analytic continuations of the functions.

By using the algebra of irreducible tensorial sets developed by Racah and others, or group theory, the matrix of the Hamiltonian for a many-electron atom, including Coulomb interaction of electrons, can be separated into distinct, nondegenerate parts which can be solved separately for their eigenvalues and eigenvectors in terms of hydrogen-like wave functions. Numerical solutions are carried out by cutting the infinite matrices down to, say, 16 x 16 matrices, which can be solved without much difficulty and given eigenvalues which are quite good for the lower energy levels. Procedures are already set up for handling atoms or ions with one, two, and three bound electrons, and no insurmountable difficulty is expected in extending them to greater numbers of electrons. Antisymmetric wave functions are used throughout.

I. ZEUS

The nine shelves of Zeus connected to Perhapsatron S-5 have been
fired at 20 kv producing over 900,000 amp peak gas current. The
Perhapsatron torus cracked during the discharge, and Zeus has not operated
while it is being rebuilt.

The transmission lines for the remaining 32 tiers have been
installed. They require fuses, switches and monitor wiring for completion.

A design for a low-inductance transmission system is under study.
It eliminates the fuses and parallel plate transmission lines and uses
cable instead. When a capacitor shorts, the cable limits the energy
into the short while the short is being sensed by a detector. The load
switches are fired immediately and most of the energy is dissipated in the
load. A computer analysis demonstrated that the design is feasible. The
system being studied will have a tier inductance of 0.035 μh and will
deliver a peak current of approximately 1 megamp. This is roughly twice
the performance of the present tier design.

TEST FACILITY

A test facility for component evaluation is being constructed. A
number of bays with protective walls have been installed. Equipment for
evaluating capacitors, cables and switches is being assembled.

The facility has voltages to 100 kv available. Two small energy
storage banks are being installed to evaluate capacitors and switches
for Sherwood application. Equipment for measuring the inductances and Q
of capacitors is also available.

COMPONENT DEVELOPMENT

A parallel plate capacitor is being developed by a commercial
laboratory. Preliminary test samples have been made to test fabrication

techniques and dielectric materials. Over 100 samples have been received and voltage tested to destruction. The best material was found to be an anti-static polyethylene known as Durathene. The tests indicate that this material has an average dielectric strength of 2 kv/mil in thickness up to 0.02 in. The dissipation factor is too low to measure on a GR-1650A bridge.

J. ULTRA-HIGH VACUUM

During the last few months an effort has been made to develop competence in modern ultra-high vacuum technology. Following the practice of the vacuum groups of other Sherwood laboratories, stainless-steel systems with oil diffusion pumps, metal gaskets, bake out at 400° to $500^{\circ}C$ and various anti-creep traps have been used. Vacua in the range of a few times 10^{-10} mm mercury are now being produced.

These vacuum systems must be capable of handling the large intermittent gas loads typical of plasma devices while at the same time keeping the base vacuum as low as possible. Contaminants in Sherwood experiments may consist of impurities adsorbed on the walls, wall materials boiled off during operation of a machine, hydrogen (or deuterium) left on the walls from previous shots, or compounds of hydrogen and wall materials formed during a shot, adsorbed on the walls and released by the next shot. It is not at all obvious that it will ever be possible to operate such machines with a really low base vacuum, but rather fast pumping systems appear to offer the best chance of success.

It has been found that in attempting to follow the recipes of other workers for producing high vacuum minor differences are frequently introduced which turn out to be of major importance in the performance of the system. In this report are listed some of the techniques which have been applied with tentative evaluation.

1) Zeolite traps, following the design of Biondi. Traps consist of optically tight baffle of three coaxial trays loaded with a thin layer of zeolite pellets. They must be baked out above $500^{\circ}C$ for 48 hours and longer to achieve vacua better than 10^{-9} mm. This may be due to a different batch of zeolite from that used by Biondi. There has been difficulty from time to time with a popcorn effect during baking, most of the pellets ending up in the diffusion pump. This was caused apparently by a batch of zeolite that had been left open for a time so as to absorb water, but some similar trouble has been had with other batches, the walls of the system near the trap ending up with a thin coating of zeolite dust. It is found that the pumping of substantial hydrogen gas bursts through the trap raises the base vacuum of the system into the 10^{-7} mm region; this is no better than conventional systems. Presumably the contaminant is hydrogen, but every background hydrogen can be inconvenient in an experiment.

2) Varian flanges with copper gaskets. Joints are usually, but not always, vacuum tight when first made up, sometimes developing leaks on baking. Some leaks appear to be due to imperfections in the copper gaskets. Other leaks are caused by relaxation of tension in the bolts on baking. Use is made of stainless 1/4 in. 20 bolts with heavy carbon steel nuts. Stainless nuts seize up on baking. Poor quality nuts deform and loosen up.

3) Welds. Where possible fusion welds made by a heliarc-type welder are used. Welds are made between two narrow lips of 347 stainless steel, machined in advance. No rod is added.

4) Non-creep Freon baffle. A non-creep Freon baffle is in use which consists of 4 copper baffle elements 1/8 in. thick, each a little larger than a semicircle. The elements are silver soldered inside a 4 in. stainless steel tube with 1/8 in. wall so as to overlap and form at least a 3 bounce baffle. The wall is Freon cooled from outside and insulated with loose vermiculite. This baffle, unbaked, is capable of holding a baked system to about 2×10^{-9} mm above a Consolidated PMC 720 pump.

5) Non-creep liquid nitrogen trap. A liquid nitrogen trap has been built employing an annular stainless steel inner container connected to the end of the trap opposite the pump by a stainless steel bellows welded in at both ends. At the end of the annulus nearest the pump is a copper baffle plate cooled by thermal conduction through copper posts. The trap is approximately a two bounce system. It has not yet been tested thoroughly, but on a system with a known leak of 8×10^{-9} cm^3 atmospheres per second it held 7×10^{-10} mm pressure above the Freon baffle and the PMC 720 pump.

6) Diffusion pumps and pump fluids. The Veeco EP41W and the Consolidated PMC 720 pumps have been used. Some difficulty was encountered with the Veeco pump in that the pressure on the high vacuum side was dependent on fore pressure to an alarming extent. This behavior may have been due to some damage done to the stack assembly when the pump was modified to use a Varian flange at the top. The PMC 720 pump has behaved very well with Convoil 20 as a pump fluid. Octoil-S has also been used and found to decompose so as to contaminate the fore pump and raise its bank-off pressure considerably. In earlier tests of the zeolite trap there appeared to be some incompatability between DC 704 pump fluid and zeolite. The system pressure is found to be higher after baking than before. The PMC 720 is a non-fractionating pump with a very large power input to immersion beaters that extend for about half their lengths above the fluid surface in the boiler. It is hard to understand how such a pump can be applicable to ultra-high vacuum, but it is and seems to behave very well.

7) Tests are underway to explore the effect on base pressure of gulps of hydrogen admitted above various cold traps as they might be during an experiment.

K. A NEW PLASMA CONFINEMENT GEOMETRY (HELIXION)

A toroidal cusped geometry, in which the large cusp losses are avoided, is based on the use of an external tight helical fold winding on the torus together with an open internal helix. The effect of this combination is to produce a chain of regions, along the axis where the field is weak, which are bounded on all sides by fields of positive curvature. (Fig. 16). In the limit of infinite conductivity, these regions can be occupied by plasma and be completely stable. However, there are cusps, such as A and C, which are bridged by a line, e.g., B, encircling the inner conductor. In the region of the bridge, the system has a curvature which is in the sense of hydromagnetic instability. It is essential to maintain stability in the bridge region and the problem resembles that of the stellerator. It is of interest to note, therefore, that the inclination of the spiral winding imparts a shear to the field in the bridge region, which should make possible a higher limiting stable value for β. Furthermore, the axial component of the current in the spiral produces a rotational transform to the axial field of the torus, as required for stability of the plasma.

A significant drawback to the system described above is that the current in the spiral must be produced by induction and so operation would be discontinuous. The concept can, however, be extended to an open-ended linear geometry, for which dc operation is possible. Consider a cusped region that could be occupied by a plasma in the vicinity of the neutral point, produced by a straight, current-carrying wire in a transverse magnetic field. Such a region has two cusps which are bridged around the wire and two cusps which connect with the outside. It turns out that as the inclination of the wire to the magnetic field is decreased, the cusped region shrinks and ultimately vanishes, without touching the wire.

For a straight, long solenoid having in it a helix (Fig. 17), the magnetic field is greatly reduced on the axis and is large between
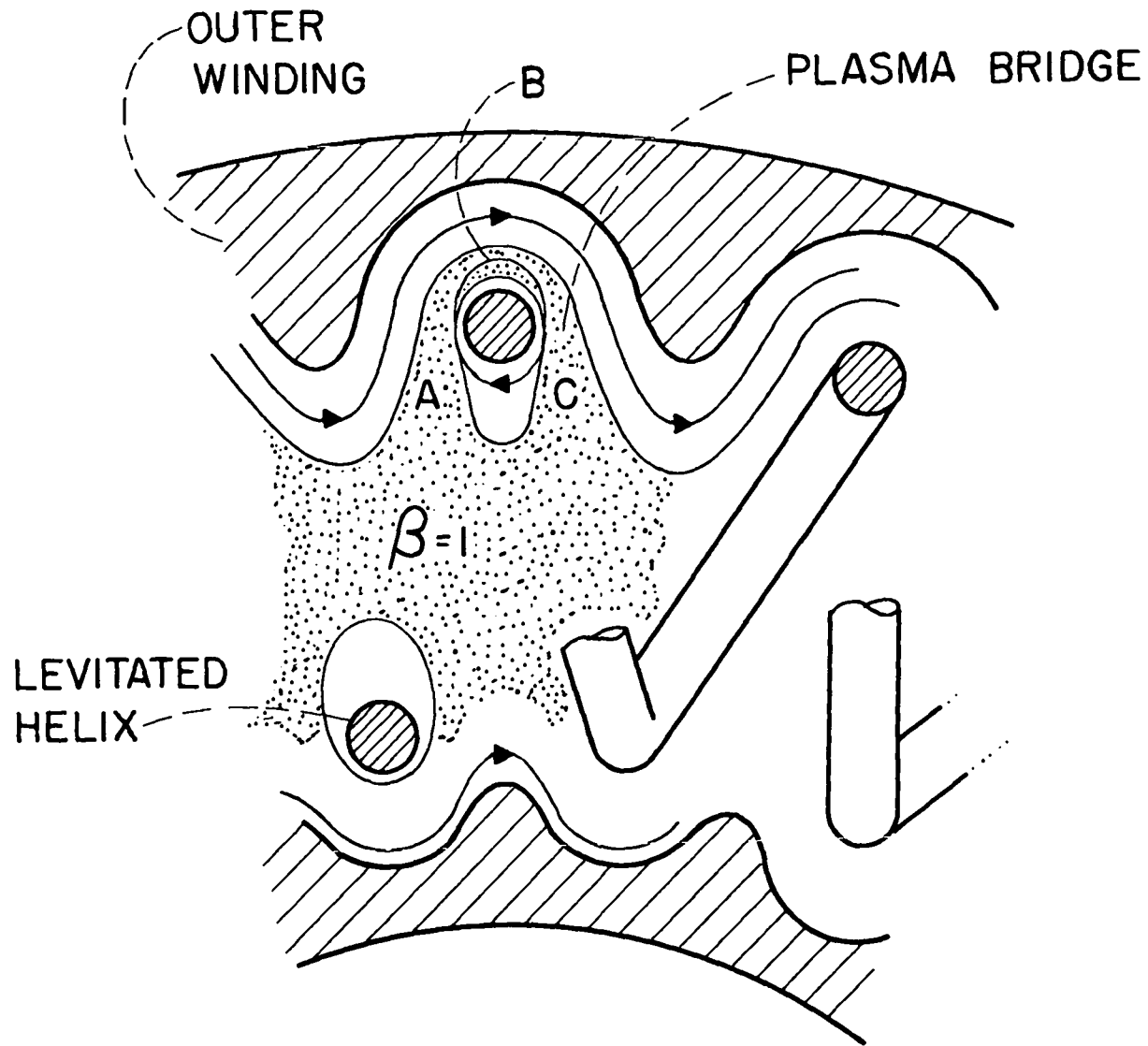
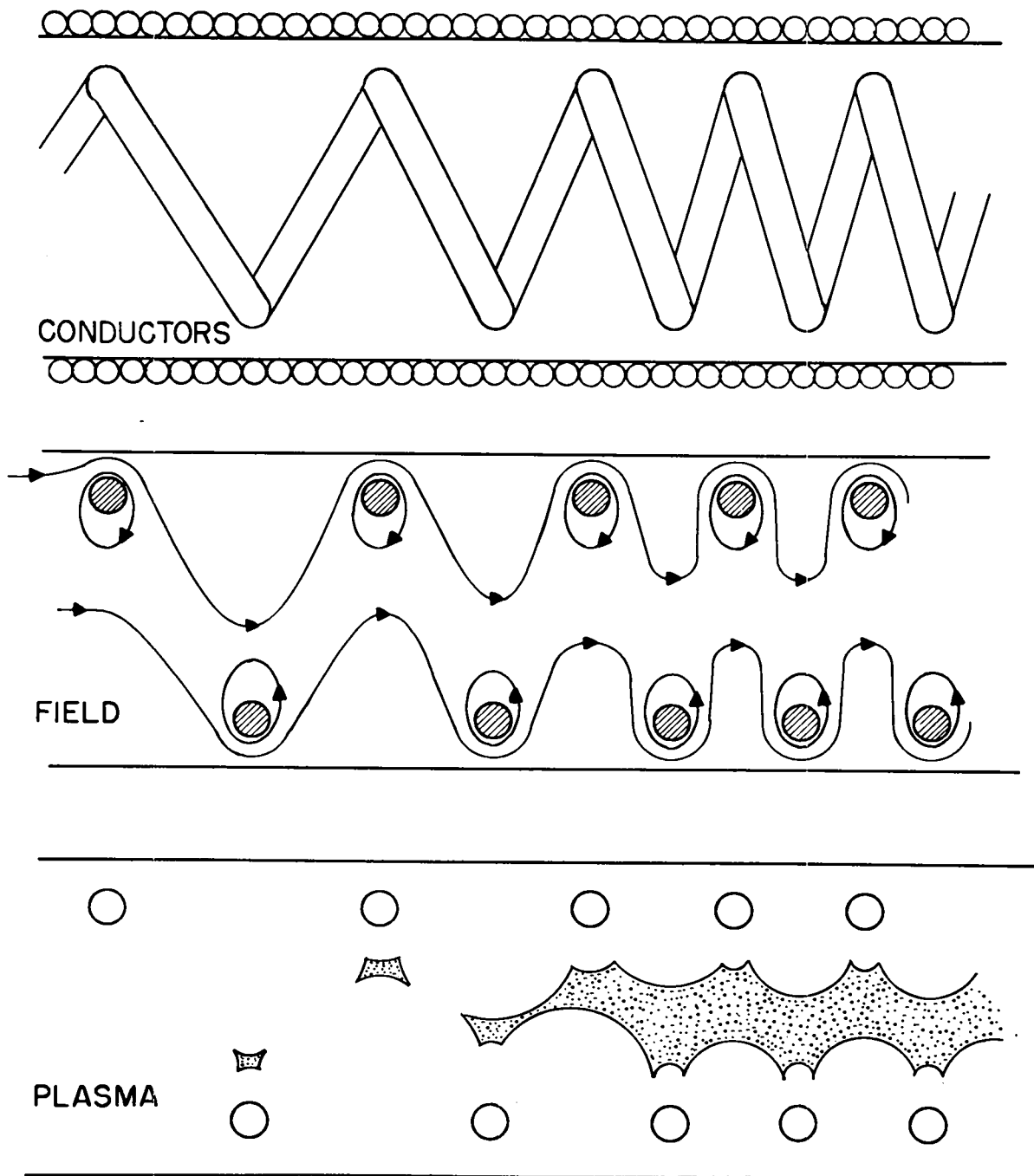Fig. 16. Helixion system in toroidal geometry

Fig. 17. Characteristics of Helixion in linear geometry

purposes, the spiral is opened up, as shown toward the left in Fig. 17, and it emerges from the end essentially as an axial conductor. The main bulk of the plasma has bridged cusps and is connected to the exterior solely at the ends via a ring cusp. Since the losses from these end cusps are independent of the length of the system, it can be made very long, with the solenoid being supported magnetically. Most, if not all, of the magnetic lines can be made to terminate at the ends of the system, so that the stream of quiescent cross-field diffusion from plasma to wall can be intercepted, at the ends, in the manner of a diverter, if desired.

The general name Helixion has been given to the proposed plasma confinement system.